# RECONSTITUTION OF A NON UNIFORM INTERFACE THERMAL RESISTANCE BY INVERSE CONDUCTION

## A. BENDADA[a],*, D. MAILLET[a], J. C. BATSALE[b] and A. DEGIOVANNI[a]

[a]*Laboratoire d'Energétique et de Mécanique Théorique et Appliquée (LEMTA), CNRS URA 875, ENSEM, 2 Avenue de la Forêt de Haye, BP 160, 54500 Vandoeuvre les Nancy, France;* [b]*Laboratoire d'Energétique et des Phénomènes de Transfert (LEPT), CNRS URA 873, ENSAM, Esplanade des Arts et Métiers, 33405 Talence, France*

Diffusive heat transfer problem within a non isotropic stratified structure, containing a plane defect of non uniform resistance, is solved analytically by the method of integral transforms. The idea consists in applying Fourier cosine transforms on the space variables and a Laplace transform on the time variable. The thermal quadrupole formalism allows to reduce the mathematical model to a product of matrices in the transformed space.

The direct modeling, within the framework of a 2D geometry, has been followed by the construction of an inverse procedure that reconstitutes the variation of the thermal resistance from the measure of the surface temperature. But in the presence of noise, this solution becomes unstable because the problem is ill-posed. To avoid an unstable solution, a method of regularization is necessary. It consists in filtering the data to make our inverse problem well-posed. The inversion can then be undertaken in an explicit way either in the transformed space, or in the real space. The established technique has been completed by a method of constrained optimization, in order to guarantee the positivity of the solution.

The developed inverse codes have been validated by noised numerical simulations and by a NDT (non destructive testing) operation by stimulated infrared thermography on a bonding defect between two PVC plates.

*Keywords:* Non destructive testing; infrared thermography; interface resistance; inverse methods; composites

---

\*Corresponding author.

## 1. INTRODUCTION

Because of the quick development of the composite material technology, mathematics problems linked to the thermal diffusion within multilayered media have been studied by many researchers. Several analytic methods have been developed, notably those using integral transforms [1, 2, 3]. The formers consist in seeking the solution not in the usual time-space domain, but in a transformed domain.

In the general case, the methods using integral transforms require a numerical processing for the calculation of the eigenvalues of the problem, the rest of the calculation being analytic. The analytic method advantage is to allow a best comprehension of the physics of transfer phenomena within the medium studied. Furthermore, these methods offer a very fast calculation when compared with numerical methods (such as finite element or finite difference methods). These numerical methods often require a very thin grid next to singularities. Nevertheless, the numerical approach remains unchallenged for the modeling of the thermal behavior of non linear systems and/or those having a complex geometry [4, 5].

The simplicity of results obtained by integral transforms methods for the resolution of the direct problem of diffusive heat transfer has allowed to develop many analytic methods for the resolution of the associated inverse problem. Applications consist in the determination of boundary conditions (of heat fluxes or of temperatures), the estimation of thermophysic properties and the determination of the geometry of a system. One often succeeds in identifying explicitly the desired parameters in the transformed space [6, 7, 8, 9, 10].

If one is interested only in the surface temperature, the thermal quadrupole formalism designed to model 1D transfer within stratified media is very practical [1]. It allows a very simple matrix handwriting linking the temporal Laplace transforms of the temperature and the flux on the face of a layer, to the same quantities on the opposite face. The matrix linking entry and exit vectors of a multilayered system is then obtained by setting all the individual matrices in series. Return in the time domain is often obtained by numerical means.

The notion of thermal quadrupole is also applicable to cases of 2D or 3D transfer [2, 3, 7, 8, 9]. The idea consists in applying to Laplace

transforms in time of the temperature and flux, new Fourier integral transforms (cartesian geometry) in one or two directions of the space. The multi-dimensional quadrupoles thus obtained have the same structure as those of 1D modeling, and are thereby used in an identical way. An interesting application of these techniques is the calculation of the transient temperature field within 2D or 3D non isotropic stratified structures comprising plane defects of complex nature.

The precise aim of this article is the illustration of the aforementioned techniques on a problem of NDT by stimulated infrared thermography of media comprising a defect of any resistance [11, 12, 13]. This type of problem is met in industrial applications (cases of delaminations in fibre reinforced materials for example). The only assumption of the model is the flatness of the defect. The direct modeling of heat conduction in the transient problem, in a 2D geometry, is followed by the construction of an inverse procedure which allows to identify the spatial distribution of the thermal resistance and its depth (uniform). The inverse problem is more arduous than the direct one because of its ill-posed character. This implies the instability of the solution caused by small variations of the data [7, 8].

## 2. PRESENTATION OF THE PROBLEM

Thermal interface resistances are the consequence of a structural discontinuity between two materials. Examples can be found in the delaminations within laminated composites or bonding defects at the interface of two media. They can be detected and possibly estimated quantitatively by using non destructive techniques. Currently, the most used method is NDT by ultrasonics. An alternative to this technique is the pulsed photothermal method, known as "flash method".

In this technique, the plate to be inspected is submitted to a heat pulse on one of its faces, while the temporal evolution of its surface temperature, either on the heated side (front face), or on the opposite side (rear face), is recorded by an infrared camera. The presence of a defect inside the material shows down heat diffusion and induces consequently a perturbation on the observed temperature field.

Thermal detection allows to measure this perturbation and to localize and characterize subsurface defects. The defect is a thermal interface resistance $R$, located at some depth $e_1$ beneath the stimulated face as shown in Figure 1.

Because of the absorption of the flash energy (absorbed energy surface density $Q$) by the slab front face, diffusion of heat in the material produces thermograms (temperature $T$ versus time $t$ curves) whose qualitative shape is shown in Figure 2a – curve $T_0^*(t^*)$ (the star superscript indicates the dimensionless quantities) for a point located on front face – and in Figure 2b – curve $T_0^*(t^*)$ for a point located on rear face – if no defect is present in the slab ($R = 0$). The presence of a defect ($R \neq 0$) will affect heat diffusion: the corresponding surface temperature – curve $T^*(t^*)$ – will decrease in a slower way (after the theoretical infinite level reached for a Dirac heat pulse) for a point located on front face – Figure 2a – while its rise will be slower on a point on rear face – Figure 2b –.

What has been described above for two different experiments ($R = 0$: sane slab, $R \neq 0$: defective slab) can also apply to the same unique slab
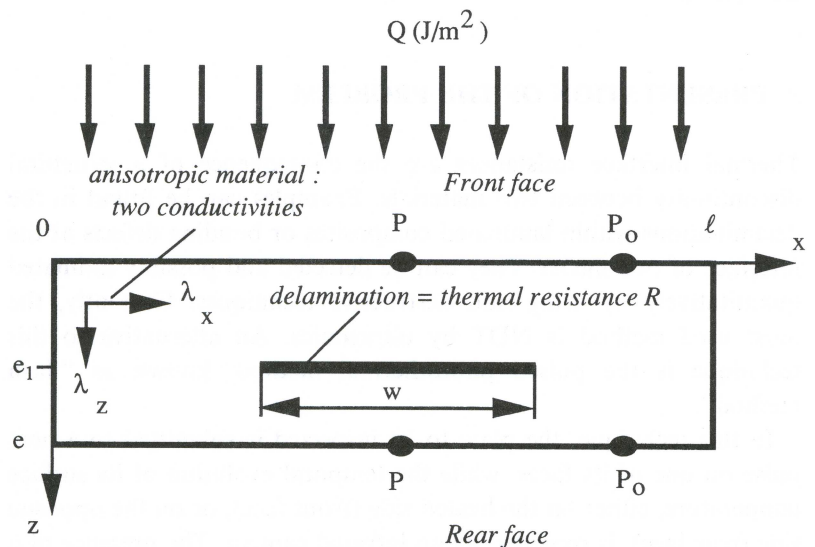


FIGURE 1 Two-dimensional problem: delamination of limited extent – all four sides insulated.

shown in Figure 1. If the sane thermogram is recorded on a point $P_0$ far from the $x$ location of the defect while the "defectuous" one corresponds to a point $P$ at the same level (same $x$) as the defect. The contrast thermogram $\Delta T^*(t^*) = T^* - T_0^*(t^*)$ constitutes therefore a signature of the defect. It is positive for front side detection (Fig. 2a) and negative for rear side detection (Fig. 2b).

## 3. TWO-DIMENSIONAL TRANSIENT HEAT CONDUCTION MODEL

The interface thermal resistance is modeled by a function of the $x$ coordinate, the diffusive heat transfer is therefore two-dimensional. This model has already been used in the case where $R$ is a piecewise constant function [2, 9, 10]. We extend it here to the more general case $R(x)$ [7, 8]. The geometry of the problem is presented in Figure 3 (cross section $x-z$ of the plate). The plate (dimensions: $\ell \times e$) is made out of an homogeneous non isotropic material, whose one of its principal directions corresponds to the $x$ axis (conductivities $\lambda_x$ and $\lambda_z$, specific heat $\rho c$).
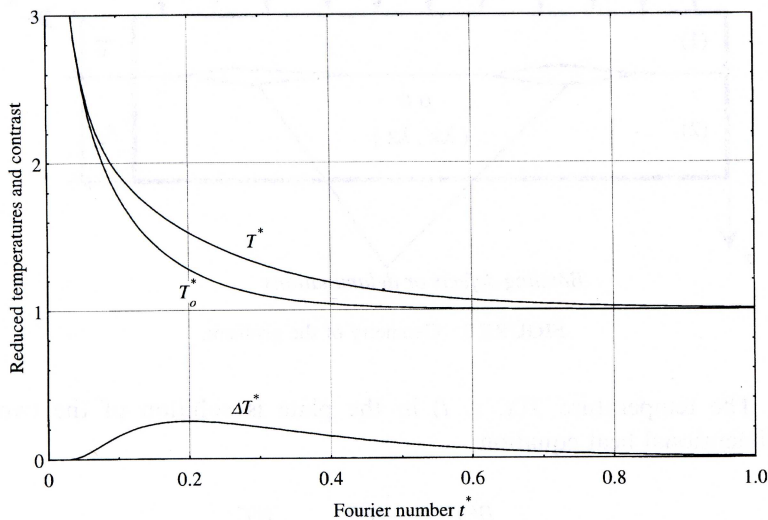


FIGURE 2a   Thermograms and contrast. One-dimensional case. *Front face.*
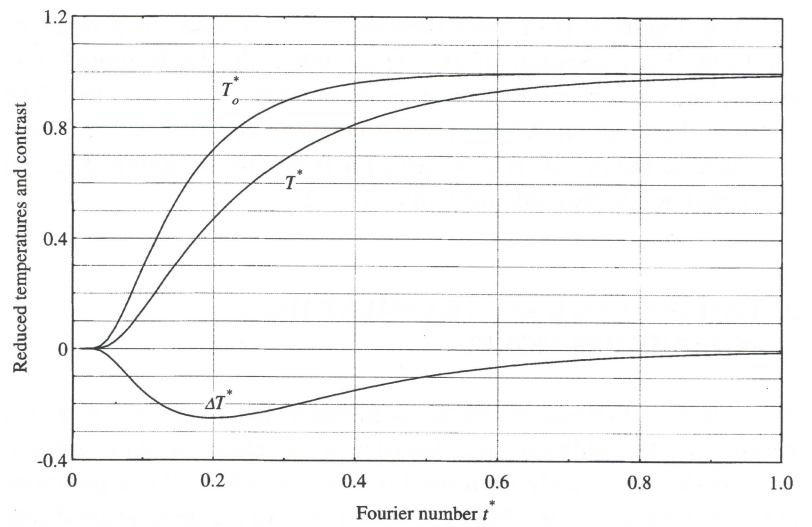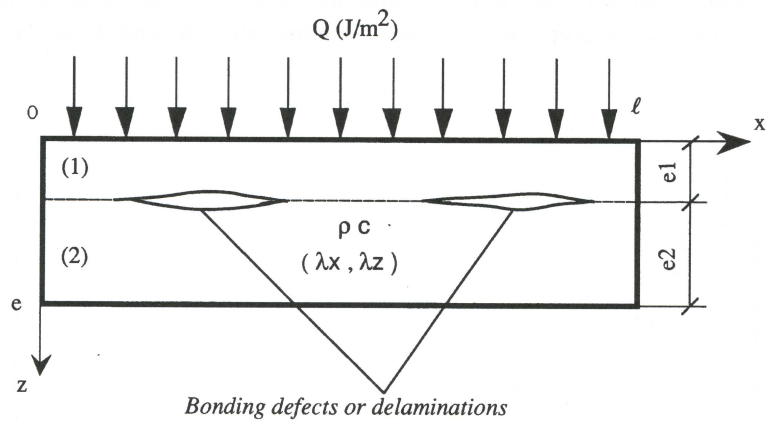
FIGURE 2b   Thermograms and contrast. One-dimensional case. *Rear face*.



FIGURE 3   Geometry of the problem.

The temperature $T(x, z, t)$ in the plate is solution of the two-dimensional heat equation:

$$\lambda_x \frac{\partial^2 T}{\partial x^2} + \lambda_z \frac{\partial^2 T}{\partial z^2} = \rho c \frac{\partial T}{\partial t} \tag{1}$$

with the following associated conditions:

- The plate temperature at initial time ($t=0$) is assumed equal to environment temperature:

$$T = 0 \tag{2}$$

- Lateral surfaces ($x=0$, $\ell$) are supposed to be insulated:

$$-\lambda_x \frac{\partial T}{\partial x} = 0 \tag{3}$$

- The density of energy $Q$ coming from a Dirac illumination pulse and absorbed by the front face ($z=0$) is taken to be uniform in space:

$$-\lambda_z \frac{\partial T}{\partial z} = Q\,\delta(t) \tag{4}$$

- The condition on the face opposite to the radiation $z=e$ is:

$$-\lambda_z \frac{\partial T}{\partial z} = 0 \tag{5}$$

- At the interface $z=e_1$, the resistance produces a temperature jump with a conservation of flux:

$$-\lambda_z \frac{\partial T^{\text{sup}}}{\partial z} = -\lambda_z \frac{\partial T^{\text{inf}}}{\partial z} \tag{6}$$

$$T^{\text{sup}} - T^{\text{inf}} = R(x) \left( -\lambda_z \frac{\partial T}{\partial z} \right) \tag{7}$$

where superscripts sup and inf relate to conditions above and beneath the resistance plane.

### 3.1. Formulation in Laplace Domain

It is possible to apply a time Laplace transform to Equation (1) and to its associated boundary, interface and initial conditions. This transform has the advantage to make the partial temporal derivative

disappear in the heat equation. The Laplace temperature $\tau$ is defined thereafter:

$$\tau(x, z, p) = \int_0^\infty \exp(-pt)\, T(x, z, t)\, dt \qquad (8)$$

The thermograms in the original temporal space can be calculated using a numerical inversion algorithm of the Laplace transform, such as Stehfest's algorithm [14].

The Laplace temperature obeys the following set of equations:

$$\frac{\lambda_x}{\lambda_z}\frac{\partial^2\tau}{\partial x^2} + \frac{\partial^2\tau}{\partial z^2} - \frac{p}{a_z}\tau = 0 \qquad (9)$$

$$\frac{\partial\tau}{\partial x} = 0 \quad \text{at} \quad x = 0, \ell \qquad (10)$$

$$-\lambda_z\frac{\partial\tau}{\partial z} = Q \quad \text{at} \quad z = 0 \qquad (11)$$

$$\frac{\partial\tau}{\partial z} = 0 \quad \text{at} \quad z = e \qquad (12)$$

$$\frac{\partial\tau^{\text{sup}}}{\partial z} = \frac{\partial\tau^{\text{inf}}}{\partial z} \quad \text{at} \quad z = e_1 \qquad (13)$$

$$\tau^{\text{sup}} - \tau^{\text{inf}} = R(x)\,\psi(x, z, p) \quad \text{at} \quad z = e_1 \qquad (14)$$

$a_z\,(=\lambda_z/\rho c)$ being the thermal diffusivity of the slab in the $z$ direction and $\psi(x, z, p)$ the axial ($z$ direction) Laplace heat flux density given by:

$$\psi(x, z, p) = -\lambda_z\frac{\partial\tau}{\partial z}. \qquad (15)$$

### 3.2. From the Non Isotropic Problem to the Equivalent Isotropic One

In order to reduce the number of parameters, it is convenient to use reduced variables:

$$\tau^* = \tau/(Qe/\lambda_z) \quad T^* = \rho ce\, T/Q$$

$$\psi^* = \psi/Q \quad \varphi^* = e^2\varphi/(a_z Q)$$

$$t^* = a_z t/e^2 \quad p^* = e^2 p/a_z$$

$$x^* = \frac{x}{e}(\lambda_z/\lambda_x)^{1/2} \quad \ell^* = \frac{\ell}{e}(\lambda_z/\lambda_x)^{1/2}$$

$$z^* = z/e \quad e_1^* = e_1/e$$

$$R^*(x^*) = R(x)/(e/\lambda_z)$$

In the following part of this article, superscript $*$ will be omitted for simplicity reasons. After this reduction of variables, the heat Equation (9) takes the following form:

$$\frac{\partial^2 \tau}{\partial x^2} + \frac{\partial^2 \tau}{\partial z^2} - p\tau = 0 \tag{16}$$

### 3.3. Formulation in Laplace-Fourier Domain

Lateral boundary conditions determine the integral transform that one has to apply to heat equation (16) in order to solve it. Its resolution by separation of variables leads to seek solutions of the type:

$$\tau(x, z, p) = \sum_{i=1}^{\infty} [A \sin(\alpha_i x) + B \cos(\alpha_i x)] [C \sinh(u_i z) + D \cosh(u, z)] \tag{17}$$

with:

$$u_i = (p + \alpha_i^2)^{1/2} \quad \text{and} \quad \alpha_i = i\pi/\ell \quad \text{with} : i \text{ natural integer} \tag{18}$$

The condition on the extremity $x=0$, determines the form of the solution by imposing the one of the two coefficients $A$ or $B$, which is non zero. In our case, the insulation condition on $x=0$ implies that

$A = 0$ and $B \neq 0$. The value of the eigenvalues $\alpha_i$ are determined by the heat insulation condition at the other extremity $x = \ell$, [15].

One undertakes afterwards the Fourier cosine spatial transform of function $\tau(x, z, p)$:

$$\theta(\alpha, z, p) = \int_0^\ell \tau(x, z, p) \cos(\alpha x) \, dx \qquad (19)$$

If $\theta$ is known, return to simple Laplace domain is given by:

$$\tau(x, z, p) = \frac{1}{\ell} \left[ \theta_{i=0} + 2 \sum_{i=1}^\infty \theta_i \cos(\alpha_i x) \right] \qquad (20)$$

with:

$$\theta_i = \theta(\alpha_i, z, p)$$

By using transformation (19) and by taking into account boundary conditions on the edges of the slab, the heat equation becomes:

$$\frac{d^2 \theta}{dz^2} - (p + \alpha^2) \theta = 0 \qquad (21)$$

One can notice that obtention of Equation (21) is made possible by the fact that one has used the eigenvalues $\alpha_i$ as particular values of the transformation variable $\alpha$ and because that boundary conditions in the $x$ direction were homogeneous. If $\phi$ is the cosine Fourier transform of the reduced Laplace flux density $\psi$, the $z$ boundary and interface ($z = e_1$) conditions become:

- Irradiated surface $z = 0$

$$\phi(\alpha, 0, p) = \frac{\sin(\alpha \ell)}{\alpha} \qquad (22)$$

- Interface $z = e_1$

$$\theta^{\sup} - \theta^{\inf} = \int_0^\ell R(x) \psi(x, z, p) \cos(\alpha x) \, dx \qquad (23)$$

- Opposite surface $z = 1$

$$\phi(\alpha, 1, p) = 0 \tag{24}$$

If $\theta(0)$, $\theta(1)$, $\phi(0)$, $\phi(1)$ are the column vectors having each $(n+1)$ components (subscripts $i = 0$ to $n$) that constitute the spectra $\theta_i$ (0 or 1) and $\phi_i$ (0 or 1) of Laplace temperature and flux density on the front or rear face, Equations (21)–(24) can be written using three matrices (of 2D quadrupoles) that stem from integration of Equation (21) with respect to $z$ [2, 7, 8]. The first two of them are associated with layers (1) and (2), respectively above and beneath the interface plane of Figure 3:

$$\begin{bmatrix} \theta(0) \\ \phi(0) \end{bmatrix} = \begin{bmatrix} A_1 & B_1 \\ C_1 & A_1 \end{bmatrix} \begin{bmatrix} \theta^{\text{sup}} \\ \phi(e_1) \end{bmatrix} \tag{25}$$

$$\begin{bmatrix} \theta^{\text{inf}} \\ \phi(e_1) \end{bmatrix} = \begin{bmatrix} A_2 & B_2 \\ C_2 & A_2 \end{bmatrix} \begin{bmatrix} \theta(1) \\ \phi(1) \end{bmatrix} \tag{26}$$

The quadrupoles in this case are block partitioned matrices, each of them being constituted by diagonal matrices of $(n+1)$ order defined by:

$$A_q = \begin{pmatrix} A_q(\alpha_0) & \cdot\cdot & \cdot\cdot & 0 \\ \cdot\cdot & A_q(\alpha_1) & \cdot\cdot & \cdot\cdot \\ \cdot\cdot & \cdot\cdot & \cdot\cdot & \cdot\cdot \\ 0 & \cdot\cdot & \cdot\cdot & A_q(\alpha_n) \end{pmatrix} \quad \text{for } q = 1 \text{ or } 2 \tag{27}$$

Diagonal matrices $B_q$, $C_q$, $D_q$ are constructed the same way:

$$A_q(\alpha_i) = \cosh(u_i e_q) \tag{28a}$$

$$B_q(\alpha_i) = \frac{1}{u_i} \sinh(u_i e_q) \tag{28b}$$

$$C_q(\alpha_i) = u_i \sinh(u_i e_q) \tag{28c}$$

with:

- $u_i = (p + \alpha_i^2)^{1/2}$ for $i = 0$ to $n$
- $e_2 = (1 - e_1)$ being the reduced thickness of the second layer.

In order to consider the complete spectra of Laplace temperatures and flux density, one should take $n = \infty$; In practice $n$ will be the number of harmonics which will be considered.

The right member of Equation (23) is in fact the convolution product (noted $*$ in Fourier domain) between the Fourier cosine transform $\rho$ of $R(x)$ and the corresponding transform $\phi(e_1)$ of the Laplace flux $\psi$ at the location of the interface: Equation (23) can be written under the ordinary form of a convolution [10]:

$$\theta_i^{\text{sup}} - \theta_i^{\text{inf}} = \frac{1}{\ell} \sum_{m=-\infty}^{m=+\infty} \rho_{i-m}\, \phi_m \tag{29}$$

If one takes into account the parity of the Fourier cosine spectrum and if one keeps only the positive harmonics, the jump of temperature at the interface under vectorial form can be written the following way:

$$\theta^{\text{sup}} - \theta^{\text{inf}} = \rho * \phi(e_1) = N_\rho\, \phi(e_1) \tag{30}$$

with:

$$N_\rho = \frac{1}{\ell} \begin{pmatrix} \rho_0 & 2\rho_1 & 2\rho_2 & .. & 2\rho_n \\ \rho_1 & \rho_0 + \rho_2 & \rho_1 + \rho_3 & .. & \rho_{n-1} + \rho_{n+1} \\ \rho_2 & \rho_1 + \rho_3 & \rho_0 + \rho_4 & .. & \rho_{n-2} + \rho_{n+2} \\ \rho_3 & \rho_2 + \rho_4 & \rho_1 + \rho_5 & .. & \rho_{n-3} + \rho_{n+3} \\ .. & .. & .. & .. & .. \\ \rho_n & \rho_{n-1} + \rho_{n+1} & \rho_{n-2} + \rho_{n+2} & .. & \rho_0 + \rho_{2n} \end{pmatrix} \tag{31}$$

$\rho$ being the column vector that contains all the components of the spectrum of $R(x)$:

$$\rho = [\rho_0\, \rho_1 \ldots \rho_n]^t \quad \text{with: } \rho_i = \int_0^\ell R(x) \cos(\alpha_i\, x)\, dx \tag{32}$$

One has now to use the flux conservation equation through the plane of the defect − transform of (13) − and Equation (30), relative to the jump of temperature at the interface. The following matrix equation is obtained:

$$\begin{bmatrix} \theta^{\text{sup}} \\ \phi(e_1) \end{bmatrix} = \begin{bmatrix} I & N_\rho \\ 0 & I \end{bmatrix} \begin{bmatrix} \theta^{\text{inf}} \\ \phi(e_1) \end{bmatrix} \tag{33}$$

$I$ and $0$ being the identity and zero matrices of order $(n+1)$.

$N_\rho$ is a convolution matrix constructed with vector $\rho$. The sums of two components of $\rho$ that appear in the majority of its elements stem from the fact that only the positive eigenvalues are considered here, since negative ones were respectively replaced by their opposite values ($\rho_{-i} = \rho_i$). The elimination of the intermediate temperature-flux vectors in the relationships (25), (26) and (33), allows to link directly conditions on front face ($z = 0$) and on rear face ($z = 1$):

$$\begin{bmatrix} \theta(0) \\ \phi(0) \end{bmatrix} = \begin{bmatrix} A_1 & B_1 \\ C_1 & A_1 \end{bmatrix} \begin{bmatrix} I & N_\rho \\ 0 & I \end{bmatrix} \begin{bmatrix} A_2 & B_2 \\ C_2 & A_2 \end{bmatrix} \begin{bmatrix} \theta(1) \\ \phi(1) \end{bmatrix} \qquad (34a)$$

This equation can be generalized for a stack of more than 2 layers separated by resistances, by superposing in series the matrices relative to all layers and all interfaces.

Since the rear face is insulated ($\phi(1) = 0$), one can find starting from Equation (34a), the rear and front face Laplace-Fourier temperature:

$$\theta(0) = (A + A_1 N_\rho C_2)(C + C_1 N_\rho C_2)^{-1} \phi(0) \qquad (34b)$$

$$\theta(1) = (C + C_1 N_\rho C_2)^{-1} \phi(0) \qquad (34c)$$

where:

$$A = A_1 A_2 + B_1 C_2 \quad \text{and} \quad C = C_1 A_2 + C_2 A_1$$

Equations (34b) and (34c) can be substracted from the corresponding equations written for $N_\rho = 0$, this gives the front and rear face contrasts, $\Delta\theta(0 \text{ or } 1)$. $\Delta\theta$ is the Laplace-Fourier transfrom of the reduced temperature difference $\Delta T$ between a point located on the face of a defectuous slab (reduced temperature $T$) and the corresponding point belonging to a sane slab (reduced temperature $T_0$ for $R(x) = 0$):

$$\Delta\theta(0) = C_2 C^{-1} N_\rho C_2 (C + C_1 N_\rho C_2)^{-1} \phi(0) \qquad (35)$$

$$\Delta\theta(1) = -(C + C_1 N_\rho C_2)^{-1} C_1 N_\rho C_2 C^{-1} \phi(0) \qquad (36)$$

where:

$$\phi(0) = [\ell \, 0 \, 0 \ldots 0]^t \quad \phi(1) = [0 \, 0 \, 0 \ldots 0]^t \qquad (37)$$

In the case where the interface thermal resistance is small with respect to the resistance of the checked specimen, simpler expressions of thermal contrasts are obtained by neglecting the product $C_1 \, N_\rho \, C_2$ in formulas (35) and (36):

- On front face:

$$\Delta\theta(\alpha_i, 0, p) = \frac{\sinh\left(e_2(p^{1/2})\right)}{\sinh\left(p^{1/2}\right)} \frac{\sinh\left(e_2 \, u_i\right)}{\sinh\left(u_i\right)} \rho_i \qquad (38)$$

- On rear face:

$$\Delta\theta(\alpha_i, 1, p) = -\frac{\sinh\left(e_2(p^{1/2})\right)}{\sinh\left(p^{1/2}\right)} \frac{\sinh\left(e_1 \, u_i\right)}{\sinh\left(u_i\right)} \rho_i \qquad (39)$$

As an example, we have shown on Figure 4 the result of a direct simulation illustrating the time-space repartition of the thermal contrast corresponding to the profile of defect thickness $e_d$ (with two humps) given by the curve in continuous line in Figure 5. The duration of the direct program does not exceed 120 seconds in CPU time on a
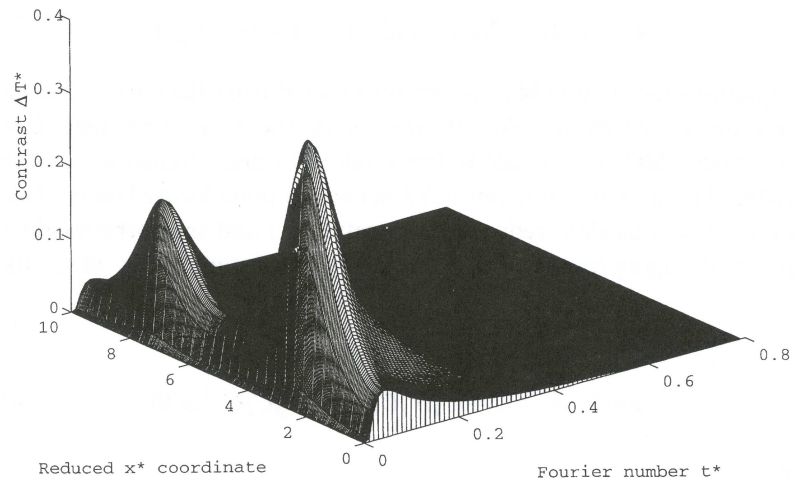


FIGURE 4   Direct simulation of thermal contrast produced by the resistance with two humps.
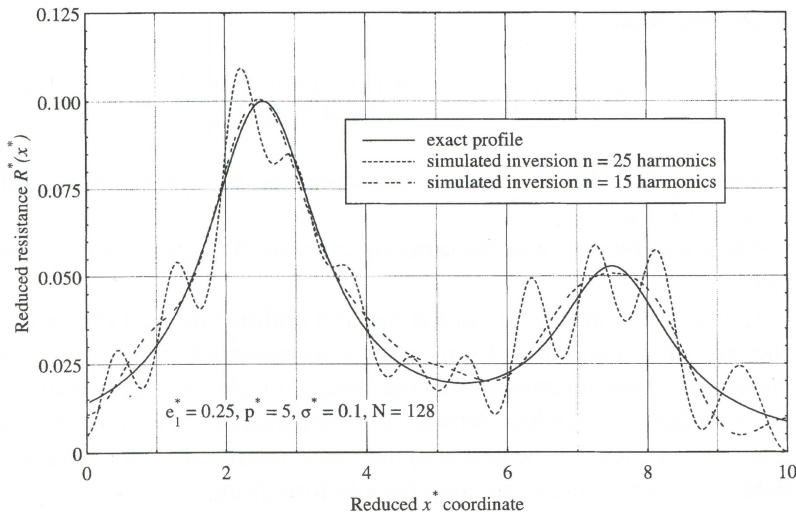
FIGURE 5 Influence of the truncation frequency on the inversion of a "smooth" resistance: (function $R^*(x)^*$ with two humps).

work station IBM RS6000-560 (128 *Mo*) for a mesh of 128 points in space and 100 points in time.

One can notice that the analytic approach for the modeling of the transfer across a 2D non uniform defect could have been extended to the 3D case (thermal resistance $R(x, y)$) by proceeding the same way: one only need to add to the term $p + \alpha^2$ of Equation (21) the square of the eigenvalue $\beta$ in the $y$ third direction, perpendicular to the $x$ axis. The difficulty appears in the handwriting of the convolution product corresponding to the jump of temperature at the interface because of coupling of modes of thermal resistance and flux density spectra. Nevertheless, in the case of defect of low resistance, the reduction of the model by the perturbation method [9, 10, 16, 17] gives the following explicit results:

- On front face:

$$\Delta\theta\left(\alpha_i, \beta_j, 0, p\right) = \frac{\sinh\left(u_{ij}\, e_2\right) \sinh\left(e_2\, p^{1/2}\right)}{\sinh\left(p^{1/2}\right) \sinh\left(u_{ij}\right)}\, \rho_{ij} \tag{40}$$

• On rear face:

$$\Delta\theta(\alpha_i, \beta_j, 1, p) = -\frac{\sinh(u_{ij} e_1) \sinh(e_2 p^{1/2})}{\sinh(p^{1/2}) \sinh(u_{ij})} \rho_{ij} \qquad (41)$$

with $\rho_{ij}$ the double Fourier transform of $R(x, y)$ function and $u_{ij} = (p + \alpha_i^2 + \beta_j^2)^{1/2}$.

These expressions have the same structure as 2D Equations (38) and (39).

In the case of defects of limited size and uniform thermal resistance, the use of integral transforms allows to construct a linear set of equations whose unknowns are components of the spectrum vector of the interface Laplace flux density. The numerical resolution of the set allows to calculate in the next step the exact superficial 3D temperature fields [2], thanks to thermal quadrupole formalism.

## 4. THERMAL RESISTANCE IMAGING

### 4.1. Explicit Inversion

The problem considered here is to estimate function $R(x)$ starting from measurement of $T(x, z = 0, t)$. Two quadratures of the measured signal, corresponding to transformation (8), with the calculation of $\tau(x, z = 0, p)$ and of the Laplace contrast $\Delta\tau(x, z = 0, p)$ and to transformation (19), allow the estimation of vector $\Delta\theta(z = 0, p)$, $p$ being any value of the reduced Laplace variable. With $N$ space points sampled (in $x$), we will evidently be able to produce no more than $N(= n + 1)$ discrete values of the spectrum $\Delta\theta$ [18]. $\Delta\theta$ is now considered as the new input signal which will be used for inversion, instead of the original one $T(x, z = 0, t)$. The difficulty of this problem stems from its strong non linearity with respect to parameter vector $\rho$. Equation (35), for front face detection, can be put under the following form:

$$N_\rho \, a = \rho * a = b \qquad (42)$$

where:

$$a = C_2 \, C^{-1} \phi(0) - C_1 \, \Delta\theta(0) \qquad (43)$$

and:

$$b = C_2 \, C_2^{-1} \, \Delta\theta(0) \tag{44}$$

The commutative property of the convolution product (42) allows to change the non linear inverse problem into a linear one as following:

$$N_a \, \rho = b \Rightarrow \rho = N_a^{-1} b \tag{45}$$

where matrix $N_a$ is constructed starting from components of vector $a$ the same way as $N_\rho$ starting from $\rho$ in its definition following Equation (31). The original distribution of the interface resistance $R(x)$ can be estimated once $\rho$ is known by resolution of Equation (45):

$$R(x) = \frac{1}{\ell} \, \rho_{i=0} + \frac{2}{\ell} \sum_{i=1}^{n} \rho_i \cos(\alpha_i x) \tag{46}$$

An alternative explicit inversion algorithm can be found if one remarks that convolution product (42) in the Fourier space corresponds to a simple product in the original space:

$$R(x) \, A(x) = B(x) \Rightarrow R(x) = B(x)/A(x) \tag{47}$$

where $A(x)$ and $B(x)$ are the originals of vectors $a$ and $b$.

In the case of low thermal resistance, the identification of spectrum $\rho$ harmonic by harmonic is immediate thanks to Equation (38). Since the resistance and experimental contrast modes are not coupled in that case. $R(x)$ is obtained by the inverse transform (46). This type of inversion seems to be very close to Lanczos method (or truncated decomposition in singular values) [18, 19, 20]. The estimation error of the spectrum is given by:

$$(e_\rho)_i = (\varepsilon_{\Delta\theta})_i / \mu_i \quad \text{for } i = 1 \text{ to } n \tag{48}$$

with : $$\mu_i = \frac{\sinh\left(e_2 \, p^{1/2}\right) \sinh\left(e_2 \, u_i\right)}{\sinh\left(p^{1/2}\right) \sinh\left(u_i\right)} \tag{49}$$

This means that too low values of the singular values $\mu_i$ (large values of $i$), will disproportionately amplify the measurement noise. A

truncation of the spectrum is then necessary in order to obtain a stable solution.

## 4.2. Summary of the Inverse Algorithm and Simulation

A large advantage of the formulation of the estimation problem in a transformed domain is the possibility to construct an inverse algorithm that is explicit and particularly fast. In order to test through simulation the above inversion algorithms, it is necessary:

- to choose the type of interface resistance $R(x)$ present in the slab,
- to generate its spectrum $\rho$ with the maximum number of harmonics $n$,
- to choose a number $N$ of equally spaced points on the $x$ axis where contrast $\Delta T$ has to be calculated for $m$ equally spaced times $t_j$,
- to calculate, for each of the $x$ points, the Laplace contrast $\Delta \tau$ for the values of $p$ that are necessary to calculate $\Delta T$ for the $m$ desired times according to Stehfest's numerical Laplace inversion algorithm [14]; Vector $\Delta \boldsymbol{\theta}$ is first calculated, for these values of $p$, according to Equation (35), once a number $n$ of harmonics has been chosen and Fourier cosine inversion allows calculation of the required $\Delta \tau$ in a way similar as Equation (20).

Once the exact $\Delta T$ solution known on the discrete points in space and time, one can:

- choose a noise-over-signal ratio characterized by a standard deviation $\sigma$, $\sigma$ is the standard deviation of a random noise that has to be added to contrast $\Delta T$ in order to generate a simulated experimental signal,
- choose the $p$ value to be used for inversion,
- implement a time quadrature (Trapezoidal rule for example) on this "experimental" contrast in order to get an "experimental" field on the front face,
- implement a space quadrature on the previous field for $n$ frequencies $\alpha_i$, in order to generate an "experimental" $\Delta \boldsymbol{\theta}(z=0, p)$ vector,
- calculate "experimental" vectors $\boldsymbol{a}$ and $\boldsymbol{b}$, given by Equations (43) and (44),
- either calculate the specturm $\rho$ by solution of system (45) and then estimate $R(x)$ using Equation (46) for the $N$ values of $x$,
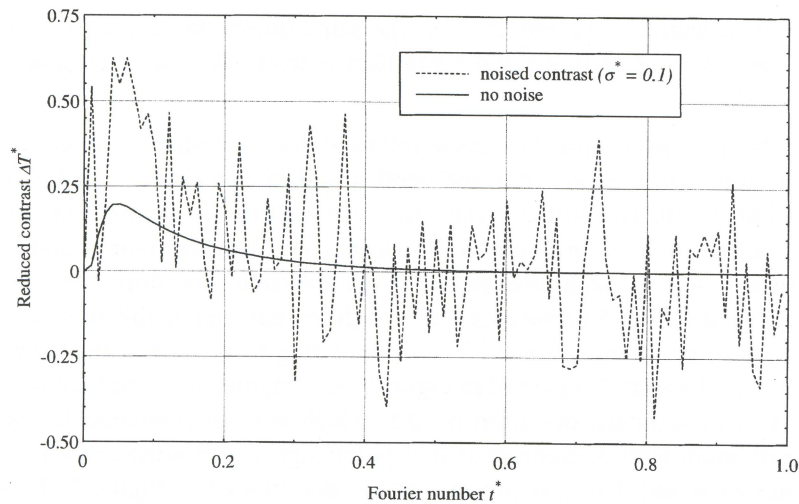
FIGURE 7   Simulated contrast thermogram at the top of the lower hump of the resistance with two humps.

noise on the estimated resistance. The methodology of its choice will be detailed later on. One remarks that the agreement seems to be very good between the true profile and that identified with $n = 5$ harmonics (errors of a few percents in comparison with $R_{max}$). The perturbation of information caused by the high frequency noise is illustrated on the profile estimated with $n = 25$ harmonics by the oscillations around the exact profile. If conversely, one uses only a few harmonics, the $R(x)$ function will be probably poorly approximated.

A similar procedure has been implemented for a piecewise constant resistance that is plotted in Figure 8 ($e_1 = 0.16$, $\ell = 9.235$). It corresponds to a square isotropic sample whose dimensional and physical properties are given in Section 6.1. The estimated profiles using the same level of noise ($\sigma = 0.1$) as before with $n = 30$ harmonics and $n = 60$ harmonics are plotted in the same figure. Inversion in this case, has been performed with the optimal Laplace variable $p = 9$ that is linked to the depth $e_1 = 0.16$. One can notice that the results are not as good as in the preceding case: it is due to the fact that a lot more harmonics are necessary to take into account the very sharp variation of the resistance in the edge of the two "doors" (Gibbs phenomena). The
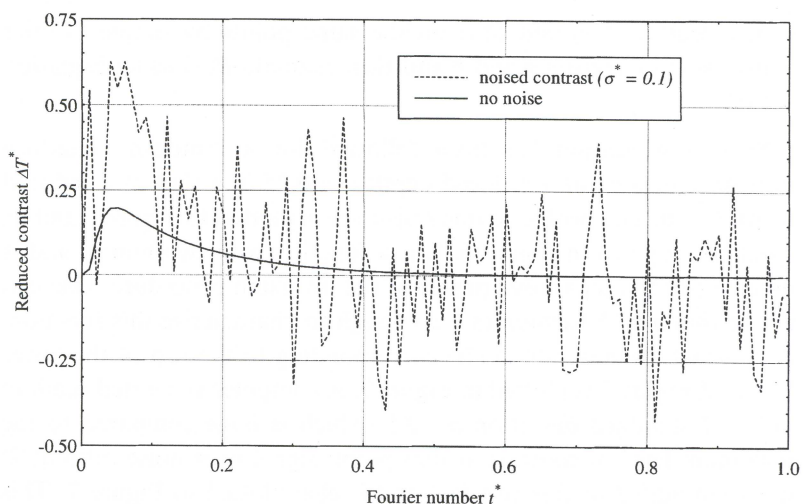
FIGURE 7  Simulated contrast thermogram at the top of the lower hump of the resistance with two humps.

noise on the estimated resistance. The methodology of its choice will be detailed later on. One remarks that the agreement seems to be very good between the true profile and that identified with $n = 5$ harmonics (errors of a few percents in comparison with $R_{max}$). The perturbation of information caused by the high frequency noise is illustrated on the profile estimated with $n = 25$ harmonics by the oscillations around the exact profile. If conversely, one uses only a few harmonics, the $R(x)$ function will be probably poorly approximated.

A similar procedure has been implemented for a piecewise constant resistance that is plotted in Figure 8 ($e_1 = 0.16$, $\ell = 9.235$). It corresponds to a square isotropic sample whose dimensional and physical properties are given in Section 6.1. The estimated profiles using the same level of noise ($\sigma = 0.1$) as before with $n = 30$ harmonics and $n = 60$ harmonics are plotted in the same figure. Inversion in this case, has been performed with the optimal Laplace variable $p = 9$ that is linked to the depth $e_1 = 0.16$. One can notice that the results are not as good as in the preceding case: it is due to the fact that a lot more harmonics are necessary to take into account the very sharp variation of the resistance in the edge of the two "doors" (Gibbs phenomena). The
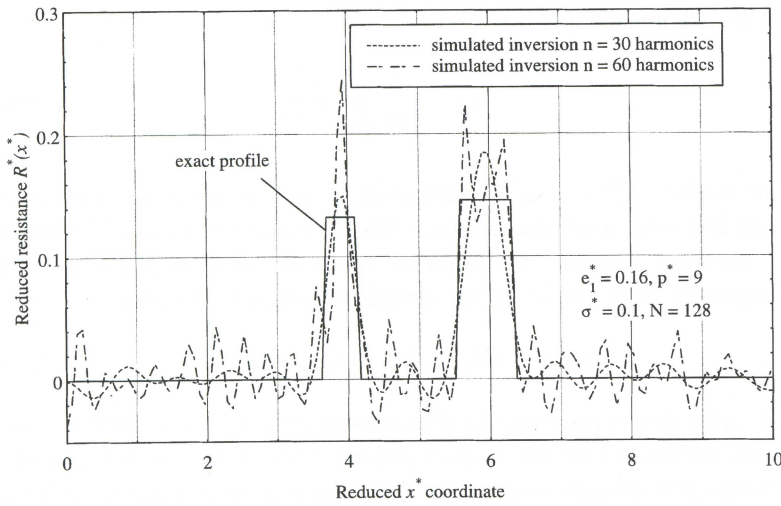
FIGURE 8 Influence of the truncation frequency on the inversion of a "hard" resistance: ("double door" $R^*(x^*)$ function).

noise has affected the significative high frequencies of the true spectrum.

### 4.3. Ill-Posed Character of the Inverse Problem

Any inversion algorithm can produce estimates of the function that is looked for. A measure of the quality of the inversion requires a compulsory estimation of the estimation error that has been made, this can be divided into three parts:

$$\|R_{n\sigma}^{Nm}(x) - R(x)\| \leq e_{\text{noise}} + e_{\text{quadrature}} + e_{\text{truncation}} \tag{50}$$

with:

$$e_{\text{noise}} = \|R_{n\sigma}^{Nm}(x) - R_{no}^{Nm}(x)\| \tag{51}$$

$$e_{\text{quadrature}} = \|R_{no}^{Nm}(x) - R_n(x)\| \tag{52}$$

$$e_{\text{truncation}} = \|R_n(x) - R(x)\| \tag{53}$$

where the norm is defined by:

$$\| \bullet \|^2 = \frac{1}{N} \sum_{k=1}^{N} (\bullet)_k^2 \tag{54}$$

and where: $R_{n\sigma}^{Nm}(x)$ is the distribution of the interface resistance identified from a thermal contrast field corrupted by an additive noise of constant standard deviation $\sigma$, space sampled in $N$ points and temporally in $m$ points, by an inversion using $n$ harmonics,

$$R_n(x) = R_{n o}^{\infty \, \infty}(x) \quad R(x) = R_{\infty \, o}^{\infty \, \infty}(x) \tag{55}$$

The error that is produced by the measurement noise $e_{\text{noise}}$ alone is the norm (calculated on the $N$ space points) of the difference between the estimated resistances with and without noise using $n$ space pulsations. The second error stems from the quadratures necessary to estimate the two transforms of the contrast on a limited number of points ($\Sigma$ instead of $\int$); This second error will be neglected as soon as $N$ and $m$ are big enough. The third error stems from the necessary truncation of the spectrum that has to be made. It will strongly depend on the shape of the $R(x)$ function: either a "smooth" function with few significative harmonics or a "harder" function as seen above.

By assuming moreover that the measurement noise on the reduced contrast $\Delta T(x, t)$ is uncorrelated, and of zero average, and that the second term in the definition of vector $a$ – Equation (43) – is negligible (which is legitimate in the case of low resistances), it is possible to determine the standard deviation $\sigma_R(x)$ of $R(x)$ created by the noise since the estimation problem is linear [21]:

$$\left(\frac{\sigma_{Rn}(x)}{\sigma}\right)^2 = \frac{\Delta t}{2Np} \left(\frac{\sinh^4(p^{1/2})}{\sinh^4(e_2 \, p^{1/2})}\right)$$
$$\times \left(1 + 2\sum_{i=1}^{n} \frac{\sinh^2((p+\alpha_i^2)^{1/2})}{\sinh^2(e_2(p+\alpha_i^2)^{1/2})} \frac{\sinh^2(e_2 \, p^{1/2})}{\sinh^2(p^{1/2})} \cos^2(\alpha_i x)\right) \tag{56}$$

$\Delta t$ being the reduced time discretization step, and quadrature being made with $N$ space points. The interest of this expression is its

independence of function $R(x)$. If one cancels the term corresponding to the summation $\Sigma$, one obtains the error of a one-dimensional inversion algorithm ($i=0$): it gives an easy way to choose a suitable value for inversion for $p$ for each depth $e_1$. It corresponds to a zero value of the derivative of this expression with respect to $e_1$. In practice, the minimum of the estimation error $\sigma_{Rn}(x)$ weakly depends of the truncation frequency $n$ and the optimal value can be chosen in a large interval close to this minimum. Consequently the optimum $p$ deduced from the 1D linear model is sufficient for the inversion of the temperature field. The evolution of Laplace variable versus the interface depth is given in Figure 9. The interest of the optimized choice of variable $p$ is illustrated by an example of simulation on the function with "two humps" in Figure 10. The inversion is carried out from a contrast affected by a noise of standard deviation $\sigma=0.1$. The optimal Laplace variable corresponding to $e_1=0.25$ is equal to 5. The identified distribution for this value is less oscillating than that inverted for $p=1$. The standard deviation $\sigma_{Rn}(x)$ is plotted in Figure 11 for the following values of the parameters: $\sigma=0.1$, $N=128$, $\Delta t=0.01$, $m=100$, $n=15$, $e_1=0.25$, $\ell=10$ and $p=5$. One can notice that the
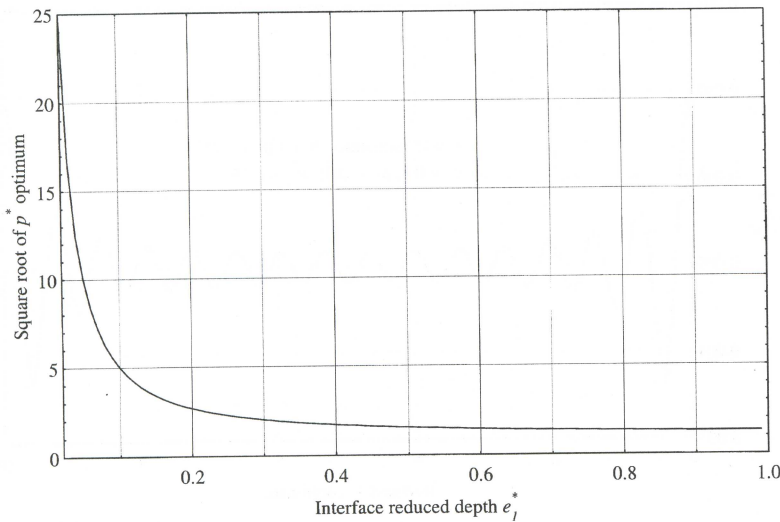


FIGURE 9   Optimal choice of the reduced Laplace variable for inversion.
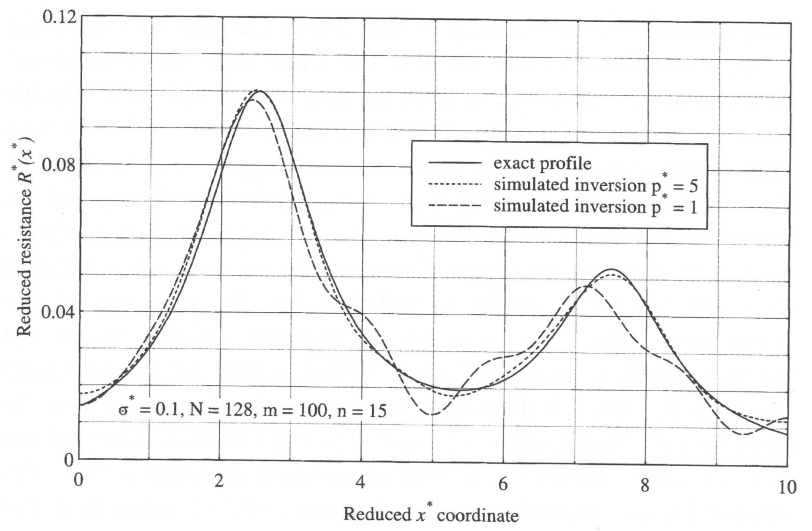
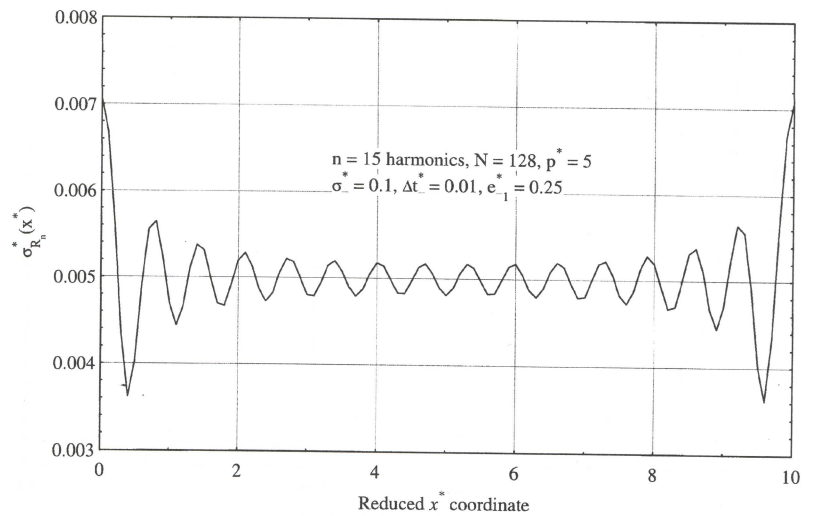FIGURE 10   Example of the influence of Laplace variable on the resistance inversion.



FIGURE 11   Profile of the standard deviation of the estimation error caused by measure noise (linearized model).

error caused by noise is about 40% higher on the edges of the sample. This stems from the fact that for the points far from the middle of the slab, the average distance of the resistance at point $x$ to the different measurement points (128 equidistant pixels) increases. The result of this, is that sensitivity of the temperature to the resistance at point $x$ becomes low, close to the edges of the sample and consequently the standard deviation becomes larger.

The variation of the norm of the standard deviation of the error caused by noise, $e_{noise}$ (linearized model), $\|\sigma_{Rn}(x)\|$, is plotted versus $n$, the number of harmonics (same values of the different constants as above) in Figure 12 (full circles). The error $e_{noise}$, calculated from inversion of a computer generated noise ($\sigma = 0.1$ and $\sigma = 0$) added to the exact contrast field corresponding to the "two humps" $R(x)$ function given in Section 4.2, is also shown on the same figure (squares): it is an increasing function of the number of harmonics and sticks to the preceding linearized curve for low values of $n$.

In order to avoid any error caused by the time and space quadratures introduced during the calculation of integral transforms used in the direct and inverse problems, the truncation error is
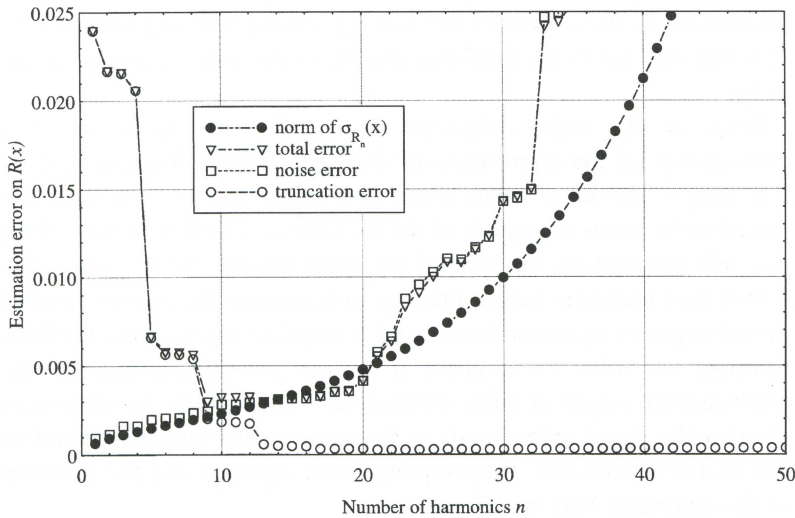


FIGURE 12   Norm of the estimation error on $R^{*}(x^{*})$ function with two humps- $\sigma^{*} = 0.1$, $p^{*} = 5$.

calculated by a simple Fourier inversion of the "theoretical" spectrum of the $R(x)$ interface resistance "with two humps". The former being calculated by a Fourier transform on a large number of points in order to get near exact values. The evolution of the truncation error is shown in Figure 12 too (empty circles): it decreases with $n$. The result of these two competitive types of errors is a total estimation error shown in the same figure (triangles) that possesses a minimum value in the $n = 10$ to $n = 18$ range. For a given interface resistance, one can therefore choose an optimal number of harmonics $n$ (which minimizes the estimation error) to invert the experimental signal. The number of harmonics $n$ is therefore a regularization parameter.

### 4.4. Regularization Techniques

#### *4.4.1. Spectrum Truncation and Wiener's Optimal Filtering*

As we have seen before, the result of high (spatial) frequency noise is that when the inverse Fourier transform is performed (following the deconvolution, system (45)), the essential features of the defect in the image (in real space) are totally obscured. It is necessary therefore to carry out one intermediate step in the inverse procedure described in Section 4.2. The idea consists in filtering out the high spatial frequencies of $\Delta\tau(x, p)$ prior to carrying out the inverse program [22]. This filtering limits the resulting quality of the sharp features in the image.

Some of the noise originates in the detector or arises as a consequence of the digitization of the signal by the imaging system. But there is also noise which arises as a consequence of the sampling linked to the space resolution of the IR camera. The former may affect not only the high components of the spectrum but the low ones too.

It is then necessary before filtering to determine the average level of the noise power spectrum (measured at negative times before the flash heating), in order to compare it to the power spectrum of the experimental signal at high frequencies. This allows to determine whether the signal corresponds to the noise in this frequency band or not. If it is not the case, the sampling is not sufficient and the accuracy of the algorithm may be affected.

A stochastic study [10] has shown that there is no correlation between the different harmonics of the experimental signal, $\Delta\theta$,

assuming an additive noise with zero mean and constant standard deviation on $\Delta T$. Under these conditions the expectancy of the measurement noise is the same for all the frequencies except the fundamental one ($i=0$). Its value is given by:

$$E[(e_{\Delta\theta})^2] = \ell \, \frac{\sigma^2 \Delta t \, \Delta x}{4p} \, (1 + \delta_{0i}) \qquad (57)$$

where $\delta_{0i}$ is Kronecker's symbol and $i$ corresponds to the harmonic $\alpha_i$.

The separation of the measured signal into signal and noise components can usefully be done "by eye" from a crude plot of power spectral density of the Laplace contrast. An improvement of the inversion can be brought by replacing the abrupt spectrum truncation by Wiener's filtering [18, 23]. By this filter, we find that we are able to remove the high frequencies and still preserve the essential features of the size and shape of the defects of interest to us. Its principle consists in applying the optimal filter $H_i$ to the measured signal in order to produce a signal that is close as possible to the true signal. The transfer function of the filter is:

$$H_i = \frac{(\Delta\theta_i)^2}{(B_i)^2 + (\Delta\theta_i)^2} \qquad (58)$$

One can note that this formula involves $\Delta\theta_i$ the true signal and $B_i$ the noise. The two of these add up to be the measured signal. One can observe also that $H_i$ will be close to unity where the noise is negligible, and close to zero where the noise is dominant. To determine Wiener's filter from Equation (58) we need some way of separately estimating $(\Delta\theta_i)^2$ and $(B_i)^2$.

The power spectrum of a measured signal will often show a signal peak sticking up above a continuous noise tail (Fig. 13). The noise spectrum is extrapolated back into the signal region as a "noise model". The measured signal power is interpolated by a smooth curve. The difference between these two curves gives the "true signal model". The quotient of the "true model" to the signal plus noise power is Wiener's filter $H_i$. The models need not be accurate for the method to be useful.
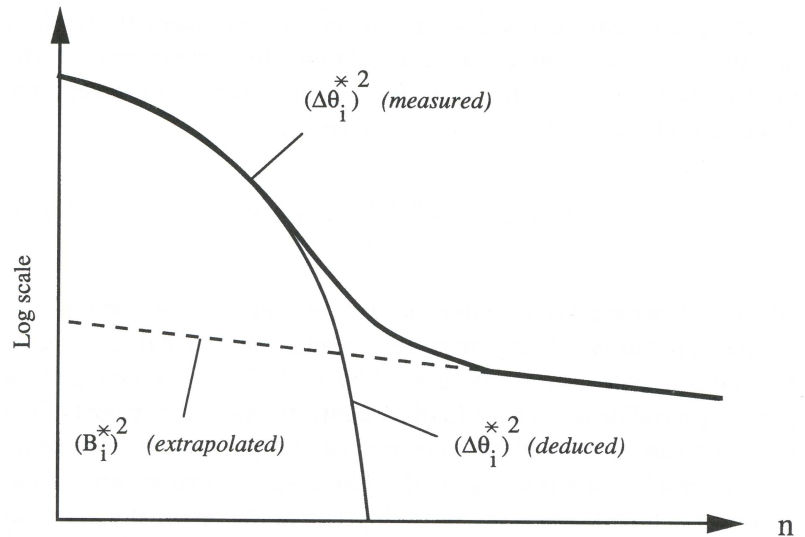
FIGURE 13   Methodology of obtention of optimal Wiener's filter.

### 4.4.2. Simulation of Inversion with Filtering

Numerical simulations, intended to test these two ways of low-pass filtering, have been performed for the inversion of the resistance with "two humps". The reduced Laplace contrast profile $\Delta\tau(p)$ has been calculated from "experimental" data described in Section 4.2 and for the Laplace variable $p = 5$ corresponding to the interface depth $e_1 = 25$. Its distribution is compared with the "uncorrupted" signal in Figure 14a. One can notice that the Laplace transformation has considerably increased the signal-over-noise ratio when compared to the original signal presented in Figure 7.

An analysis of the power spectrum of the "measured" signal has shown that the part corresponding to the noise is flat and it spreads on a large band of frequencies [10]. The useful part of the signal spreads on a small region in the proximity of the origin, and is constituted approximately by 15 harmonics. This number corresponds to the significative frequencies of the true $\rho$ spectrum given in Figure 6. A truncation window at this level seems to be adequate for the regularization of the inversion (Fig. 14b).
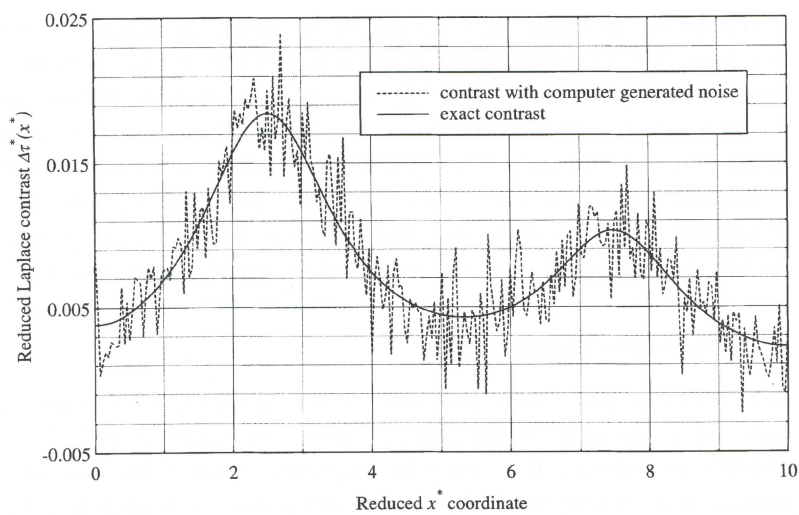
FIGURE 14a   Exact and noised Laplace contrast profiles produced by the interface resistance with two humps ($p^* = 5$, $\sigma^* = 0.1$).
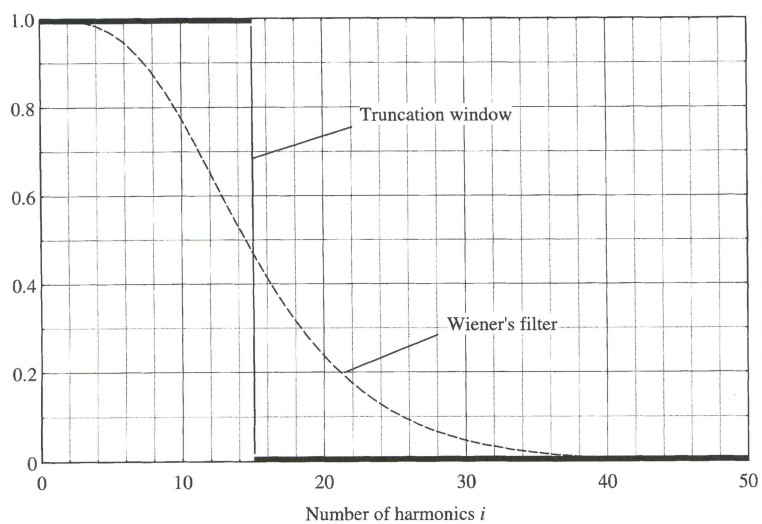


FIGURE 14b   Truncation window and Wiener's filter in the case of the interface resistance with two humps.

Thanks to the procedure described in the preceding paragraph, we have been able to determine the transfer function of Wiener's optimal filter that is given in Figure 14b too. It is a strongly decreasing function, which cancels at the forteith harmonic. Profiles identified by truncation and Wiener's filtering are compared to the exact profile (continuous line) in Figure 14c. Results obtained by the two techniques are equivalent and close enough to the exact profile, despite the fact that it concerns a case where the resistance is low.

### 4.4.3. Equivalent Defects Method

The inversion procedures described above, generate local negative resistances, especially in the case of "hard" functions (Fig. 8). It is possible to improve the result by imposing constraints. The idea consists in estimating in the first time, the interface resistance $\hat{R}(x)$ by the algorithm described in paragraph 4.4.1. According to the number of humps which appear in the identified distribution, one looks for an interface resistance constituted by the same number of square defects, in the second time. Each defect is characterized by these parameters:
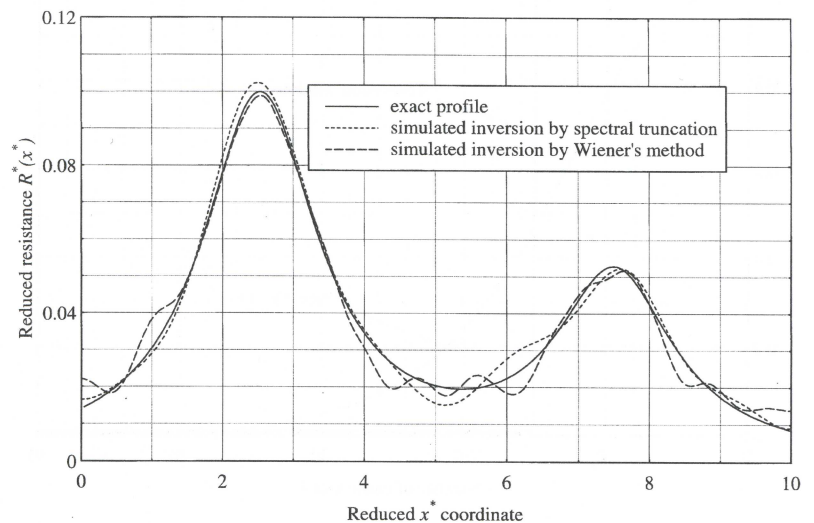


FIGURE 14c   Comparison of truncation and Wiener's methods.

its level $R$, its size $b$ and its position $x_m$. One replaces thus, the problem of function estimation by a problem of parameter estimation. These new parameters must make this piecewise constant function the closest to the estimated function $\hat{R}(x)$, in the least square sense. Thanks to Parseval's theorem, the sum of the quadratic mean deviations to be minimized can be written in Fourier domain:

$$(\hat{R}, \hat{x}_m, \hat{b}) = Arg\left( \min\left( \sum_{k=0}^{n} (\tilde{\rho}_i - \rho_i(R, x_m, b))^2 \right) \right) \qquad (59)$$

where: $\hat{R}, \hat{x}_m, \hat{b}$ are the parameter vectors to be estimated.

$\tilde{\rho}_i$ is the spectrum estimated by the filtering procedure.

$\rho_i$ is the analytical spectrum of the piecewise constant function.

The initialization of the unknown parameters is carried out using the local maxima of the estimated resistance $\hat{R}(x)$: the defect resistance $R_k$ correspond to the amplitudes of these maxima, while their centers $(x_m)_k$ to their locations. The lateral extensions $b_k$ correspond to points characterized by 40% of the amplitude of the maxima, on each side of them [6]. This choice of the initial parameters makes the convergence of the optimization algorithm (simplex method) easier: too far values from the parameters may lead to diverging results.

Numerical simulations have been performed to validate this technique on the function with "two humps". The minimum level of the resistance has been reduced to zero in this six parameter model. The method gives equivalent parameters representative enough of the real distribution (Fig. 15). This new global approach, can be very efficient in the industrial field where the first criteria consist in thresholds of tolerance for defects thickness and size.

## 5. DEFECT DEPTH IMAGING

The determination of a simple analytic expression allowing the identification of the interface depth from the non linear Equation (35) seems to be difficult. Nevertheless, one can obtain a set of equations whose the only unknown is the depth $e_1$ by eliminating the
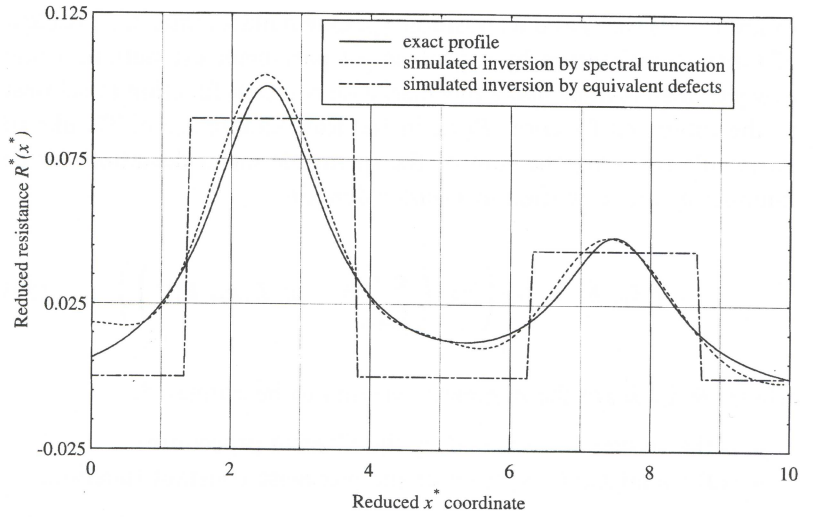
**FIGURE 15** Estimation of the function $R^*(x^*)$ with two humps and estimation of the two pieces closest to this function.

presence of $R(x)$ from Equation (47). By writing the equation for two distinct values of the variable $p$, one obtains:

$$\frac{B(x, p_1, e_1)}{A(x, p_1, e_1)} = \frac{B(x, p_2, e_1)}{A(x, p_2, e_1)} \tag{60}$$

The interface depth can then be determined by solving the set of equations using the non linear least square method on the totality of pixels $x_i$ of the experimental thermal contrast:

$$\hat{e}_1 = \text{Arg}\left(\min\left(\sum_{x_i}\left(\frac{B(x_i, p_1, e_1)}{A(x_i, p_1, e_1)} - \frac{B(x_i, p_2, e_1)}{A(x_i, p_2, e_1)}\right)^2\right)\right) \tag{61}$$

The initialization of the optimization can be performed by a first estimation of the interface depth from the linear model (Eq. 38) written for the fundamental mode ($\alpha = 0$):

$$\Delta\theta(0, 0, p) = \frac{\sinh^2(e_2 p^{1/2})}{\sinh^2(p^{1/2})}\rho_o \tag{62}$$

If one notes $\bar{R}$ and $\overline{\Delta\tau(0,p)}$ the respective spatial averages of the function $R(x)$ and the reduced Laplace contrast $\Delta\tau(0, x, p)$, the preceding expression becomes:

$$\overline{\Delta\tau(0,p)} = \frac{\sinh^2(e_2\,p^{1/2})}{\sinh^2(p^{1/2})}\,\bar{R} \tag{63}$$

If one writes this relationship for two distinct values $p_1$ and $p_2$ of Laplace variable $p$ (with $p_2 = 4\,p_1$), one can eliminate the parameter $\bar{R}$. If one confuses the two space average experimental Laplace contrasts $m_1$ and $m_2$ (calculated from the recorded temperature field using Eq. (8)) with their theoretical equivalents $\overline{\Delta\tau(0, p_1)}$ and $\overline{\Delta\tau(0, p_2)}$, an analytic expression of the depth, function of $m_1$ and $m_2$ is available:

$$\begin{aligned}
(\hat{e}_1)_{\min} = 1 - \frac{1}{(p_1)^{1/2}} \times \ell n \Bigg( &\left(\frac{m_2}{m_1}\right)^{1/2} \cosh\left((p_1)^{1/2}\right) \\
&+ \left(\left(\frac{m_2}{m_1}\right)\cosh^2((p_1)^{1/2}) - 1\right)^{1/2}\Bigg)
\end{aligned} \tag{64}$$

Stemming from the linear model, this value can be very close to the true one in the case of defects of low resistances or for those that are close to one of the two faces of the test slab ($C_1 N_\rho C_2$ negligible in formula (35)).

The preceding procedure have been performed for the smooth resistance described in Section 4.2 ($e_1 = 0.250$). Thanks to Equation (64), we obtain an approximate value of the interface depth: $(\hat{e}_1)_{\text{init}} = 0.270$. An improvement of this solution is brought using the optimization Equation (61): $\hat{e}_1 = 0.233$. Although the artificial thermal signal $\Delta T$ used for inversion was very noised ($\sigma = 0.1$), this result is very satisfactory (local error $\Delta R(x) = 7\%$).

To study the influence of a bad estimation of the depth on the resistance inverse problem, we have done simulations starting from the not noised data shown in Figure 4 [10]. The "two humps" function identified using the exact depth $e_1 = 0.25$ is very close to the true resistance. However, a 20% error $\Delta e_1$ on the depth implies a 30% local error $\Delta R(x)$ on the resistance.

Apart from the interface depth, the eigenvalues of the problem are also assumed to be known in the resistance inversion program. A bad

estimation of the thermal conductivities of the material constituting the sample, or a bad measurement of its dimensions introduces a mistake on the reduced width $\ell$ and consequently on the eigenvalues (see Section 3.2). As for the depth, we have simulated starting from the same data as above, the influence of this error on the identified $R(x)$; A 10% error on the reduced width has practically no impact on the inversion results [10].

Another factor which can introduce an error on the estimated quantities is the choice of the reference zone. Effectively, observing the infrared frame and selecting the same region is a flawed approach. In the context of a linear model, we have been able to analyze the effect of a bad choice of the undisturbed data. If the "sane zone" is in reality defective and admits $R_0$ as thermal resistance, one shows [10] that the estimated $R$ is in fact an over-resistance with respect to $R_0$: $R = R_d - R_0$ ($R_d$ being the real resistance of the defect). On the other hand, one shows that there is no error on the estimated depth $e_1$ [10].

## 6. EXPERIMENTAL VALIDATION

### 6.1. Description of the Experiment

In practice, it is very difficult to calibrate an artificial defect of known characteristics. A thermal resistance profile with "two doors" has been realized by sticking two PVC square plates. The bonding has been insured by an adhesive film that has been deposited on the whole interface except two parallel bands, creating thus a piecewise constant thickness of air $e_d(\ell = 58 \text{ mm}, e = 6.28 \text{ mm}, e_1 = 1 \text{ mm}, \rho c = 1.327$ $10^6 \text{ Jm}^{-3}\text{K}^1, a_x = a_z = 1.248 \ 10^{-7} \text{ m}^2 \text{ s}^{-1})$ and therefore a thermal interface resistance profile $[e_d(x) = (\lambda_d/\lambda)e R(x)$ with $\lambda_d = \lambda_{\text{air}} = 0.026$ W m$^{-1}$K$^{-1}$]. The thickness profile has been measured by an optical way (first door: thickness = 0.144 mm for a width of 3 mm, second door: thickness = 0.159 mm for a width of 5 mm) [10]. These values have been chosen in such a way that 2D effects of heat transfer are important enough [24]. The distribution of the defect thickness is shown in Figure 17b (curve 1). The reduced values correspond to $e_1 = 0.16, \ell = 9.235$ (same dimensions as in paragraph 4.2). The rear faces of the sample have been coated with a black paint in order to get high uniform emissivity and absorptivity.

The temperature field on the front face of the two-layered specimen (vertical) was recorded by a short wave infrared analyzer AGEMA 782 SW. Heat pulse excitation was produced by an assembly of four flash tubes located on the sides of a 10 cm vertical square. The duration of the photothermal radiation corresponds to a few milliseconds for an incident energy $Q$ of 3 to 4 J cm$^{-2}$. The IR analyzer endowed with a DATAMIN acquisition system, has been used to produce, to digitize and to store the thermographic signal. After the falsh heating, the IR frames have been recorded during 149.76 s with a period of 0.64 s. The side of the sample corresponds to 120 pixels on the IR images.

Figure 16 displays a frame of the sample in absolute temperature 5.12 s after the flash, time when the thermal contrast on the largest stripe is at its maximum. A quick inspection of this thermographic image allows easily to choose a sane zone, where internal defect presence cannot be found. It is the set of pixels delimited by a rectangle on the infrared image. This zone will be used later for the calculation of the thermal contrast, which constitutes the entry signal of the inverse methods. In practice, the normalization of the temperature field is done on a local basis: it considers an absorbed energy $Q$ at the level of $P$ that may differ from the corresponding quantity at point $P_0$ on the same face. This operation has also the advantage of completely cancelling the effect of space varying distribution of the absorptivity on the front face (flash band) and of the emissivity of the measured face (IR sensor).

In front face detection, for insulating materials (which is the case here), the Biot number of heat losses is important, and the asymptotic level at the end of the thermogram does not exist. In a such case, the asymptotic adiabatic temperature in each point, can be evaluated at the short times of the relaxation temperature curve. Indeed, the thermogram at that times obeys to the model of a semi-infinite sane medium [10]. If one calls $T_s$ the dimensional temperature at point $P$ recorded immediately after the flash heating – at dimensional time $t_s$ of the first frame for example –, one has:

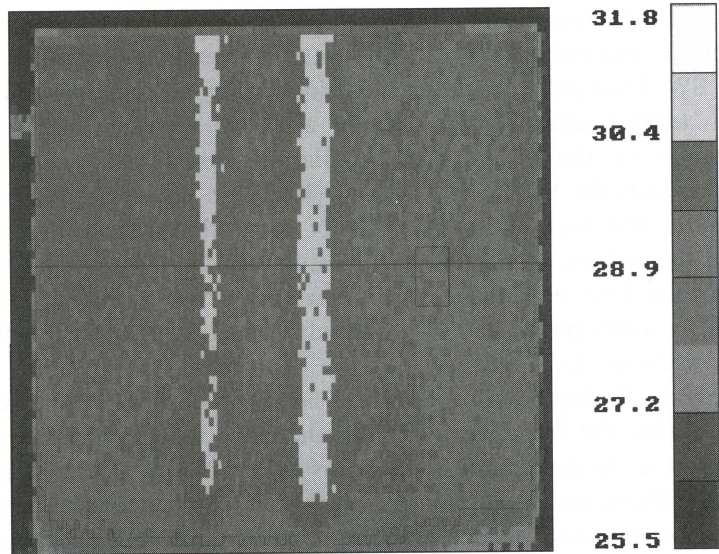$$T_s = \frac{Q}{(\pi \lambda_z \rho c t_s)^{1/2}} \qquad (65a)$$

**FIGURE 16** Thermographic frame ($T$ (°C)) at $t = 5.12$ s after the flash heating: time when the contrast on the largest defect is at its maximum. (See Color Plate I).

If the experiment was adiabatic, one would have for a same local excitation $Q$:

$$T_\infty = \frac{Q}{\rho c e} \tag{65b}$$

By elimination of $Q$ between relationsheeps (65a) and (65b), one obtains:

$$T_\infty = T_s (\pi t_s^*)^{1/2} \tag{65c}$$

where $t_s^*$ is the Fourier number corresponding to time $t_s$. The evaluation of $T_{0\infty}$ at point $P_0$ is done the same way starting from the temperature $T_{0s}$ at that point at time $t_s$. One can then calculate the local contrast by another way:

$$\Delta T_{\text{loc}}^* = \frac{1}{(\pi t_s^*)^{1/2}} \left( \frac{T}{T_s} - \frac{T_0}{T_{0s}} \right) = T^* - T_0^* \tag{65d}$$

This new formula allows to produce a contrast very close to the one without heat losses. One can note that the depth is obviously known in this case, since it is equal to the thickness of the first layer ($e_1 = 1$ mm). It will be nevertheless estimated by the procedure described in Section 5, in order to test its performance. Furthermore, the spatial distribution of the thermal resistance will be identified by the different inverse methods developed.

## 6.2. Experimental Interface Resistance Identification

In this section, we will compare the merits of the different inversion techniques using the experimental data of line 30 indicated on the temperature frame of Figure 16. The interface depth will be set to its exact value that is $e_1 = 0.16$. The value of the corresponding optimal Laplace variable is $p = 9$. The Laplace contrast profile calculated with this value is shown in Figure 17a. One remarks that on the sample edges, the signal varies brutally. This can be explained either by heat losses on these extremities, or by a non uniform energy deposit on the front face.

The power spectrum of the thermal contrast has shown that the measurement noise predominates above the thirtieth frequency. A
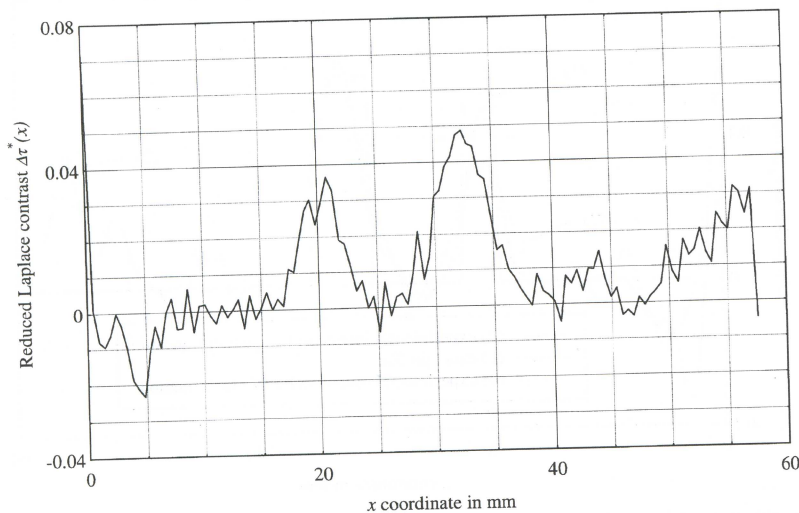


FIGURE 17a   Laplace contrast profile calculated with $p^* = 9$.

truncation window selecting the first thirty harmonics seems to be appropriate to take into account the useful part of the experimental profile, although the exact spectrum is rich in higher space frequencies. The transfer function of Wiener's filter stemming from the spectral study of the experimental data, is calculated according to Equation (58).

The distribution obtained from an inversion with $n = 30$ harmonics (curve 2) is compared to this exact profile (curve 1) in Figure 17b. The distribution corresponding to an inversion using Wiener's filter (curve 3) is shown in the same figure. The agreement between the profile identified by the two 2D techniques and the exact distribution seems satisfactory, except for the values obtained next to the boundaries (probably an effect of a non uniform flash stimulation) and the levels of maxima of the two "doors". The two kinds of low-pass filtering used give close enough results.

One can notice that the 2D spectral inversion procedure used is not based on any assumption on the function to be estimated, except the number of harmonics that has to represent it. The function $R(x)$ is defined by a set of scalars (a finite number of eigenvalues) only. In our
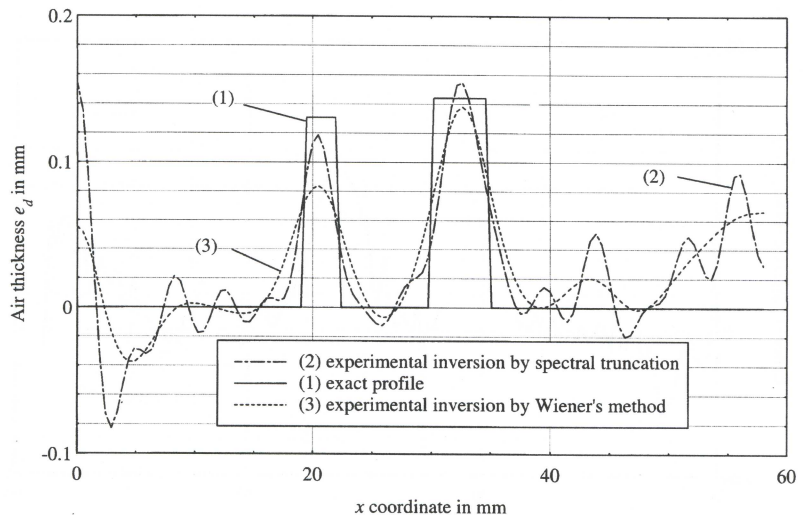


FIGURE 17b    Profile of defect thickness: experimental inversion by truncation ($n = 30$ harmonics) and Wiener's techniques.

opinion, that constitutes an important advantage on other inversion procedures, like Tikhonov regularization method [25], which requires the adjustment of two a priori arbitrary parameters: the number of pieces that is going to represent the dicretized function and the regularization coefficient. Of course, in practice, a general function can not be accurately estimated from any given data. In our problem, the space resolution on $R(x)$ depends on the space resolution of the infrared camera.

## 6.3. Experimental Inversion Using Equivalent Defects Method

The consideration of a priori hypothesis, which can be formulated starting from the rough profile (2) of Figure 17b alone: " the resistance $R(x)$ is a function constituted only of two non zero pieces", allows, by the equivalent defects method described in Section 4.4.3, to determine the six parameters characterizing the two "doors". The derived distribution – Figure 18 – is very close of the exact distribution although it concerns low thermal resistances.
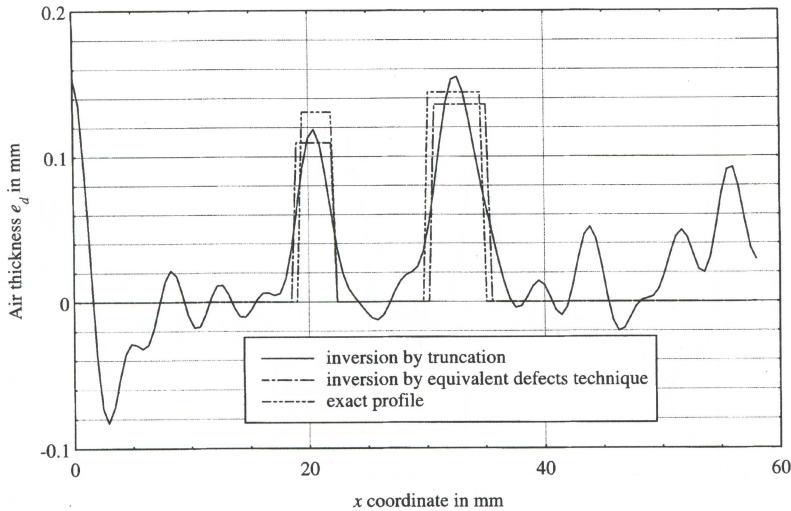


FIGURE 18   Profile of defect thickness: estimation of a function (truncation $n = 30$) and estimation of the two pieces closest to this function.

## 6.4. Comparison with 1D Algorithm

The comparison of results obtained by the 2D spectrum truncation method and by the 1D inverse technique, is illustrated in Figure 19. The 1D inverse problem is solved analytically and assumes that the defect and plate widths are infinite with a uniform thermal resistance [6]. One can see clearly that there is no large difference between the spatial evolutions of the two identified functions.

This does not mean that 2D phenomena are non-existent, but one can explain it by the fact that the elimination of the high spatial frequencies has decreased the spatial resolution of the procedure in such a way that one no longer distinguishes the advantage brought by 2D modeling.

Infact, during non noised simulations, this anomaly does not appear, because all the harmonics until Shanon frequency have been taken into account. The advantage that brings the 2D modeling is then observable (Fig. 20). This advantage can become significant during experimental data processing, if the signal-over-noise ratio is good enough. This would be possible by using the new IR matricial cameras which offer an accuracy of about 0.01°C.
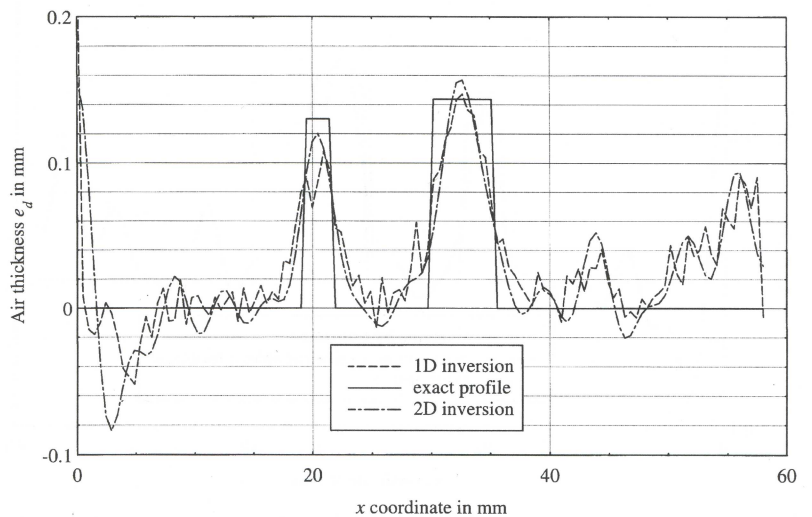


FIGURE 19   Profile of defect thickness: comparison between 1D and 2D inversions.
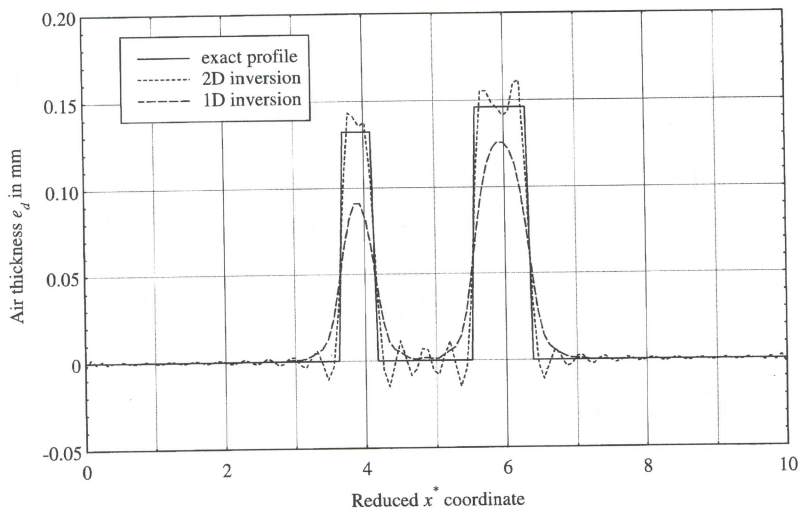
FIGURE 20    Profile of defect thickness: comparison by simulation between 1D and 2D inversions of true data.

It is interesting to note that the profiles in Figure 19 have been obtained by processing only a single line of each frame of the thermographic film. The average of twenty lines ( possible here because the $y$ direction does not intervene) allows to recognize the square aspect of the two doors (improvement of the signal-over-noise ratio) – Figure 21 –.

Another way to reduce the effect of the noise is to stimulate the sample with a more large energy $Q$. This operation would be very interesting especially for very deep defects for which contrasts are very weak. However, it should not be forgotten that with very high energy the sample is risked to be burned up; Which is very far from the objective of a NDT operation.

## 6.5. Experimental Interface Depth Identification

The determination of the interface depth has required the calculation of two spatial profiles of the reduced Laplace contrast for two different values of the reduced variable $p$ ($p_1 = 1$ and $p_2 = 4$). The implementation of the depth inverse algorithm gives a first estimation of the reduced value $(\hat{e}_1)_{init} = 0.076$, thanks to Equation (64). This first
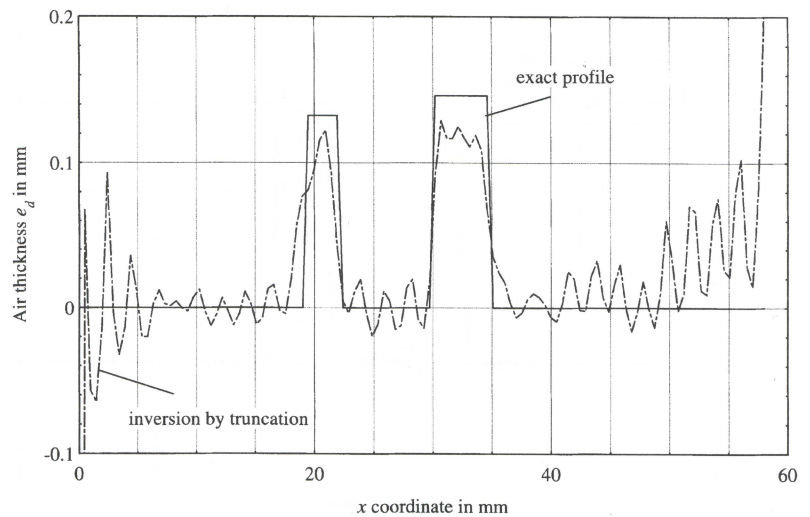
FIGURE 21  Profile of defect thickness: experimental identification by truncation ($n = 60$ harmonics), average of 20 lines.

identification has been used for the initialization of a least square method to approach more closely the true depth $e_1 = 0.160$ ($= 1$ mm). The processing yields a final value $\hat{e}_1 = 0.115$, which corresponds to 0.725 mm depth. The inaccuracy of this result is doubtless due to the abnormal shape of the temperature field next to the vertical sides of the specimen (Fig. 17a).

A simulation on the same resistance distribution has been carried out starting from a computer generated noised contrast $\Delta T(\sigma = 0.1)$. This time, the approximate value of the depth is $(\hat{e}_1)_{init} = 0.127$ and the final identified one is $\hat{e}_1 = 0.147$. The former is very close of the true depth.

## 7. CONCLUSION

The use of analytic methods based on integral transforms in time and in space has allowed to model the transient heat diffusion through a non uniform plane defect, in a plate of simple geometry. The problem has been solved using a simple enough mathematical formalism that

takes into account the non uniform interface resistance (2D thermal quadrupole). In NDT by stimulated infrared thermography, the use of these same integral transforms, calculated this time from the recorded temperature field, allows to characterize the defect in an explicit and fast way.

The tomographic approach for non uniform defect characterization described in the course of this work, could have be extended to 3D case (thermal resistance $R(x, y)$) by proceeding the same way. The difficulty lies of course in the writing of the convolution product because the coupling of thermal resistance and interface heat flux density modes. In order to discard this difficulty, analytic approximative techniques such as perturbations method [9, 10, 16, 17] joined to the assumption of separability of the double spectrum, could have give a first approximation of the solution. The former will be able to be refined thereafter by analytic or numerical methods.

In industrial applications the calculation time may be a very important factor. It is interesting to notice that a combination of the 1D method – Figure 19 – with the method of the equivalent defects, can be very effective since it represents a very good compromise between precision and calculation time. The 1D inversion is ten time more rapid than that taking into account 2D phenomena.

One can note finally that the characterization method described in this paper, in addition to its rapidity and its accuracy, offers the possibility to be applied in-situ and notably when the access is difficult or limited to a single side of the slab to be inspected (front face process). Furthermore, the new technology of matricial analyzers, which offers a high frame frequency, will allow to extend NDT by infrared thermography to thin and therefore rapid materials (metallic slab welding, thin coating, etc...). However, this technique has a disadvantage of being not very sensitive to deep defects or for the bad heat conductors.

### References

[1] Degiovanni, A. (1988). Conduction dans un mur multicouche avec sources: extension de la notion de quadripôle, *International Journal of Heat and Mass Transfer*, **31**, 553–557.
[2] Batsale, J. C., Maillet, D. and Degiovanni, A. (1994). Extension de la méthode des quadripôles thermiques à l'aide de transformations intégrales – Calcul d'un

transfert thermique au travers d'un défaut plan, *International Journal of Heat and Mass Transfer*, **37**(1), 111–127.

[3] Leturcq, Ph., Dorkel, J. M., Ratolojanarhary, F. E. and Tounsi, S. (1993). A two-port network formalism for 3D heat conduction analysis in multilayered media, *International Journal of Heat and Mass Transfer*, **36**(9), 2317–2326.

[4] Ramos, F. M. (1992). Résolution d'un problème inverse multidimensionnel de diffusion par la méthode des éléments analytiques et par le principe de l'entropie maximale: contribution à la caractérisation de défauts internes, Thesis, Ecole Nationale Supérieure de l'Aéronautique et l'Espace, France.

[5] Raynaud, M. and Bransier, J. (1986). A new finite difference method for the non linear inverse heat conduction problem, *Numerical Heat Transfer*, **10**, 27–42.

[6] Maillet, D., Houlbert, A. S., Didierjean, S., Lamine, A. S. and Degiovanni, A. (1993). Non-destructive thermal evaluation of delaminations in a laminate. Identification by measurement of a thermal contrast (Part I). The experimental Laplace transform method (Part II), *Composites Science and Technology*, **47**, 137–172.

[7] Bendada, A., Batsale, J. C., Degiovanni, A. and Maillet, D. (1994). Interface resistances: the inverse problem for the transient thermal technique, *Inverse Problems in Engineering Mechanics* (Proc. ISIP 94), Balkema, Rotterdam, NL, pp. 347–354.

[8] Maillet, D., Batsale, J. C., Bendada, A. and Degiovanni, A. (1996). Méthodes intégrales et contrôle non destructif par thermographie infrarouge stimulée, Revue Générale de Thermique, **35**, 14–27.

[9] Batsale, J. C., Bendada, A., Degiovanni, A. and Maillet, D. (1993). Distribution of a thermal contact resistance: inversion using experimental Laplace and Fourier transformations and an asymptotic expansion, *Proc. 1st International Conference on Inverse problems in engineering*, Palm Coast, ASME New York, pp. 139–145.

[10] Bendada, A. (1995). Tomographie infrarouge stimulée Estimation d'une résistance d'interface non uniforme, Thesis, Institut National Polytechnique de Lorraine, France.

[11] Balageas, D., Krapez, J. C. and Cielo, P. (1986). Pulsed photothermal modeling of layered materials, *J. Appl. Phys.*, **59**, 348–357.

[12] Cielo, P., Maldague, X., Deom, A. and Lewark, R. (1987). Thermographic non destructive evaluation of industrial materials and structures, *Mater. Eval.*, **45**, 452–466.

[13] Vavilov, V. P. and Taylor, R. (1982). Research Techniques in NDT, 5th edn. Academic Press, London.

[14] Stehfest, H. (1970). Remarks on algorithm 368, Numerical inversion of Laplace transforms, *Comm. A.C.M*, **13**, 47–49.

[15] Carslaw, H. S. and Jaeger, J. C. (1959). Conduction of Heat in Solids. Clarendon Press, Oxford.

[16] Aziz, A. and Na, T. (1984). Perturbations Methods in Heat Transfer, Springer, Berlin.

[17] Hagen, K. D. (1987). A solution to unsteady conduction in periodically layered, composite media using a perturbation method, Technical note, *Trans. A. S. M. E. J. Heat Transfer*, **109**, 1021–1023.

[18] Press, W. H., Flannery, B. P., Teukolsky, S. A. and Vetterling, W. T. (1989). Numerical recipes, Cambridge University Press, London.

[19] Linz, P. (1994). A new numerical method for ill-posed problems, *Inverse Problems*, **10**(1), L1–L6.

[20] Golub, G. H. and Van Loan, C. F. (1989). Matrix computations, second edition, Ed Jhons Hopkins University Press, Baltimore and London.

[21] Beck, J. V. and Arnold, K. J. (1977). Parameter estimation in engineering and science, John Wiley and Sons, New York.

[22] Murio, A. D. (1993). The mollification method and the numerical solution of ill-posed problems, Wiley interscience publication.

[23] Thomas, R. L., Favro, L. D., Crowther, D. J. and Kuo, P. K. (1992). Inversion of thermal wave infrared images, Eurotherm conference n°27, Proc. QIRT'92, pp. 278–282.

[24] Lamine, A. S. (1988). Caractérisation de défauts dans les matériaux composites par thermographie infrarouge, Thesis, Institut National Polytechnique de Lorraine, France.

[25] Tikhonov, A. N. and Arsenine, V. Y. (1977). Solution of ill-posed problems, V. H. Winston and Sons, Washington, D. C.